Modeling the Plasma Actuator via the Splitting of the Electric Potential

I.H. Ibrahim
PhD Student, Thermal and Fluids Division
NTU
Singapore
im0001im@ntu.edu.sg

M.Skote
Assistant Professor, Thermal and Fluids Division
NTU
Singapore
mskote@ntu.edu.sg

***Abstract*— An attempt is made to capture the effects of different magnitudes of plasma actuation in the positive and negative slopes of the applied voltage. The Suzen-Huang plasma actuator model is further improved by the addition of a posterior DC sinusoidal function that powers the actuator. The resulting body forces show that further experimental benchmarks are required to justify the accuracy of the improved model.**

Keywords- plasma actuator, flow control, Debye length

I. INTRODUCTION

All models require a coupling of the 'plasma' equations with the 'flow' equations [1-7]. The Lorentz force is used to couple the resultant force produced by the charges to the source terms in the Navier-Stokes equations.

Two forms of modeling of the plasma actuator can be derived from existing modeling techniques: the microscopic [1, 4, 7] and macroscopic form [2, 5-6]. The microscopic form evolved from the 'fluid' model described in present industrial plasma simulations. The present plasma actuator model captures the motion of the charge particles by coupling the drift-diffusion equation with the Maxwell equation. The macroscopic form captures the essential physics of the flow by modeling the electric potential characteristics as well as defining the charge density that forms the Lorentz force.

A macroscopic model is able to capture plasma induced effects on the fluid domain of a model, while a microscopic model allows the understanding of motion of individual charged particles during a plasma actuation cycle. The lesser computing requirements in investigating the macroscopic models are more appealing for such simulations to be a part a design stage for a iterative optimization concept of plasma actuator applications, as mentioned in Corke T.C., et al. [8].

It was with this notion that the Suzen-Huang actuator model [6] was chosen because although it was a macroscopic model, the modeling technique allowed the visualization of the formation of charged densities, a feature which is similar to a microscopic model. The technique has been applied to turbine blades [6, 9-10] to achieve reduction in flow separation. A 3-D analysis has also been studied [11].

A. Details of the Suzen-Huang Model

The Suzen-Huang model had its roots in concept of electroosmotic flow [12]. Electroosmotic flow refers to the motion of fluid induced by the presence of an applied voltage in a capillary tube or narrow channel. The mathematical equation derived from the flow is based on the division of the electric potentials into two forms: one via the charge density, one via the surface of the walls. The body force term is obtained by multiplying the two terms. By coupling the necessary electromagnetic and hydrodynamic equations, modeling of the plasma actuator can be conducted.

Core to the modeling of the plasma actuator is to determine a plasma characteristic length, or the Debye length λ_D. Essentially, λ_D determines whether body forces come into play or not. Oppositely charged particles in the plasma cloud interact with each other to form body forces. The mobility and hence temperature and density of the particles are related to their Debye length which are also directly correlated to the body force.

The model consists of two asymmetrically placed electrodes separated by a dielectric material as shown in Figure 1. An alternating voltage source is applied to the top electrode, while the bottom electrode is grounded. The asymmetric electrode design results in a body force that induces the flow in the direction from the exposed electrode toward the covered electrode. The geometry in Figure 1 is used in investigations done in Orlov D.M. and T.C. Corke [5].

II. METHODOLOGY

The two dimensional incompressible Navier Stokes equation can be modeled in COMSOL [13] solved using a body force F_b included in the momentum equation. The solutions from the equations are the two velocity components u and v in the horizontal and vertical directions respectively.

The body force vectors are calculated from the Lorentz equation. The Lorentz force can be written as:

$$\boldsymbol{F_b} = \rho_c \boldsymbol{E} \tag{1}$$

where $\boldsymbol{F_b}$ is the Lorentz body force, ρ_c is the charge density and $\boldsymbol{E}$ is the electric field.

The system is assumed as quasi-steady because of the nature of plasma formation and its overall effect to the fluid system. The basis of the Suzen-Huang model is the decoupling of the electric potential Φ into two parts; one under the influence by the electric field (ϕ), and the other

by the surface walls (φ). It follows from the assumption that if the Debye length is small enough, the distribution of the charge particles are only governed by the potential on the walls and unaffected by the electric field. The physics of this separation was derived for electroosmotic flow and had been initiated by Henry D.C. [12]. Numerical modeling of electroosmotic flow [14] to justify this assumption.

The Lorentz Force in equation (1) can be further expressed as:

$$\boldsymbol{F_b} = \rho_c \left(-\nabla \phi\right) \tag{2}$$

The Suzen-Huang model requires determining the variables ρ_c and ϕ. The simulation domain in its final non-dimensionalised form is shown in Figure 2.

A DC sinusoidal term *f* (t) is included in the expression of the non-dimensionalised charged density, ρ_c* via

$$\rho_c^* = \rho_{c,\max} f\left(t\right) \tag{3}$$

where is *f(t)* is defined as:

$$f\left(t\right) = \left|\sin\left(2\Pi\omega t\right)\right| \tag{4}$$

ω refers to the frequency of the voltage supply in Hz.

The function includes an absolute sign which is similar to computational works done in Likhanskii A.V., et al. [15] where repetitive short pulses with DC bias are imposed on the actuator. This is different from previous studies by Suzen [6, 9-11] where a time-dependent function is coupled in both the upper and lower electrodes. The addition of the absolute sign results in the production of the positive body force in the direction towards the surface of the lower electrode, similar to that obtained in previous studies. It will be seen later that this term will be multiplied by a posterior time function that enables the model to capture of different body forces within the positive and negative cycles of the sine function.

The characteristic λ_D used in industrial plasma engineering [16] is approximately $1.7\text{x}10^{-4}$ m. The maximum charged density, $\rho_{c,max}$, is set as 0.0075 C/m^3 as used in a previous simulation [10].

The system used is a Dell workstation model E5520 with dual quad-core processors running at 2.26GHz. The workstation has 24GB of installed memory (RAM) and used Windows 7 Professional as its operating system.

The simulations are solved using the finite element computational package, COMSOL Multiphysics^{TM} 3.5. The computing package allowed the pre- and post-processing stages of the investigations to be conducted simply in the single program. The geometry of the plasma actuator is initially drawn and meshed in an unstructured fashion. The size of the elements near the electrodes is kept within the characteristic Debye length.

The simulations are initially solved in steady state, but with parametric increments of φ_{max} to reach a value of 5 kV. The solution is then used as an initial condition to the time-dependent investigation. This solving technique is similar to that used in a previous plasma modeling investigation [10]. The parametric and time-dependent simulations took a total maximum time of 10530 CPU seconds.

III. VALIDATION OF RESULTS

Simulation results are compared with experimental data gathered in Jacob J.D, et al. [17]. In particular, two figures are compared: the streamline and velocity profile plots. The figures represent the induced velocities on a quiescent environment that had been conducted in the experiment.

Figure 3 shows the non-dimensionalised electrical potential φ^* comparison with simulations done in GHOST [10] and COMSOL. The comparisons show good general agreement in both results. The contours are more crowded near the gap of the electrodes and spreads out evenly further away from the electrodes. The curvatures of the streamline become more pronounced at the surface of the lower electrode, indicating the general direction of the body force.

The maximum induced velocities obtained by the simulations are compared to the experimental values. The u velocity profiles for this simulation show good agreement in terms of downstream strength and jet thickness, but still are not as strong as the observed experimental flow at the most downstream location of 1.6 cm from the exposed electrode interface. These velocity profiles also over-predict the contribution of the u component of the body force near the electrode interface.

Subsequently, the two parameters of λ_D and $\rho_{c,max}$ are 'tuned' to obtain a more accurate data interpretation of the plasma actuator. The Debye length, λ_D is set at $5\text{x}10^{-3}$ m while the maximum charge density $\rho_{c,max}$ is 0.0005 C/m^3. The result shows that the u velocity profiles for this simulation show better agreement in terms of downstream strength and jet thickness, but still are not as strong as the observed experimental flow at the most downstream location of 1.6 cm from the exposed electrode interface. Also for the v-velocity, a maximum negative velocity for the v component is observed at the interface.

IV. ADDITION OF A POSTERIOR TIME-DEPENDENT FUNCTION

A plasma actuator is powered by an AC voltage and the discharge behaves differently for both positive and negative half cycles of a sine wave [4, 15, 18-19]. The alternating cycle results in two 'pushes' on the fluid domain. Due to the self-limiting structure of the plasma actuator, the first 'push' is larger than second. This had been verified experimentally [18-19]. Based from the studies, a modification of the DC bias term in equation (4) is done and imposed on the encapsulated electrode boundary condition ρ_c, as:

$$\begin{aligned} f\left(t\right) &= 0.5a\left\{\left|\sin\left(2\Pi\omega t\right)\right| + \sin\left(2\Pi\omega t\right)\right\} \\ &+0.25b\left\{\left|\sin\left(2\Pi\omega t\right)\right| - \sin\left(2\Pi\omega t\right)\right\} \end{aligned} \tag{5}$$

where a =1
b = 0.3
ω =1

The values of a and b are taken from the ratios of maximum corresponding plasma densities as observed in

Enloe C.L., et al.[18] in the ‘positive’ and ‘negative’ half cycles. The resultant force propagation resembles two absolute sine functions with different peaks, as shown in Figure 7. When the plasma actuator is operating in the positive cycle of the sine wave, the cathode is position above the dielectric. The opposite happens when the actuator is in the negative cycle.

V. Conclusion

The Suzen-Huang model a charge density term multiplied with a DC sinusoidal function to induce a body force into a quiescent medium. The results show that the charge density has to be more expansive within the domain of the neutral fluid, on top of the encapsulated electrode. It can be seen that the resulting manipulation of the body force vectors results in a more entrained fluid profile similar to that observed experimentally.

An attempt to link the microscopic and macroscopic plasma actuator models is made by a posterior addition of the time function to the input charge density equation. The result shows that the ratios of the maximum observed charge density do not correspond to in a similar ratio of the maximum induced body forces. While this non-linearity can be a natural phenomenon, further investigations resulting from the body force time-evolution plasma actuation are required to substantiate the accuracy of the present model.

References

[1] Massines, F., et al., *Experimental and theoretical study of a glow discharge at atmospheric pressure controlled by dielectric barrier.* Journal of Applied Physics, 1998. **83**(6): p. 2950-2957.

[2] Roth, J.R., D.M. Sherman, and S.P. Wilkinson. *Boundary layer flow control with a one atmosphere uniform glow discharge surface plasma*. in *36th Aerospace Sciences Meeting & Exhibit.* 1998. Reno, Nevada.

[3] Shyy, W., B. Jayaraman, and A. Andersson, *Modeling of glow discharge-induced fluid dynamics.* Journal of Applied Physics, 2002. **92**(11): p. 6434-6443.

[4] Boeuf, J.P. and L.C. Pitchford, *Electrohydrodynamic force and aerodynamic flow acceleration in surface dielectric barrier discharge.* Journal of Applied Physics, 2005. **97**(10): p. 1-10.

[5] Orlov, D.M. and T.C. Corke. *Numerical simulation of aerodynamic plasma actuator effects*. in *43rd AIAA Aerospace Sciences Meeting and Exhibit - Meeting Papers*. 2005.

[6] Suzen, Y.B., et al., *Numerical simulations of plasma based flow control applications*, in *35th AIAA Fluid Dynamics Conference and Exhibit*. 2005. p. 1-11.

[7] Rouffet, J.-B. *Plasma Actuator Influence on Air Flow*. in *COMSOL Conference 2008*. 2008. Hannover: COMSOL.

[8] Corke, T.C., M.L. Post, and D.M. Orlov, *Single Dielectric Barrier Discharge Plasma Enhanced Aerodynamics: Physics, Modeling and Applications (Review Article).* Experimental Fluids, 2009(46): p. 1-26.

[9] Suzen, Y.B. and P.G. Huang. *Simulations of flow separation control using plasma actuators*. in *44th AIAA Aerospace Sciences Meeting and Exhibit AIAA 2006-877*. 2006. Nero, Nevada.

[10] Suzen, Y.B., P.G. Huang, and D.E. Ashpis, *Numerical simulations of flow separation control in low-pressure turbines using plasma actuators*, in *45th AIAA Aerospace Sciences Meeting*. 2007: Toronto, Ontario Canada. p. 11358-11365.

[11] Reasor Jr, D.A., R.P. LeBeau Jr, and Y.B. Suzen. *Unstructured grid simulations of plasma actuator models*. in *Collection of Technical Papers - 37th AIAA Fluid Dynamics Conference AIAA 2007-3973*. 2007. Miami, Florida.

[12] Henry, D.C., *The Cataphoresis of Suspended Particles. Part I. The Equation of Cataphoresis.* Proceedings of the Royal Society of London. Series A, Containing Papers of a Mathematical and Physical Character, 1931. **133**(821): p. 106 - 129.

[13] COMSOL, *COMSOL Multiphysics Modeling Guide*, in *COMSOL 3.5a*. 2008.

[14] Patankar, N.A. and H.H. Hu, *Numerical Simulation of Electroosmotic Flow.* Analytical Chemistry, 1998(70): p. 1870-1881.

[15] Likhanskii, A.V., et al. *Modeling of interaction between weakly ionized near-surface plasmas and gas flow*. in *44th AIAA Aerospace Sciences Meeting and Exhibit (AIAA 2006-1204)*. 2006. Reno, Nevada.

[16] Roth, J.R., *DC Electrical Glow Discharge in Gases*, in *Industrial Plasma Engineering Volume 1: Principles*. 1995, Institute of Physics Publishing p. 284-351.

[17] Jacob, J.D., et al. *Control of Laminar and Turbulent Shear Flows Using Plasma Actuators*. in *4th International Symposium on Turbulence and Shear Flow Phenomena*. 2005. Williamsburg, VA.

[18] Enloe, C.L., et al., *Mechanisms and Responses of a Single Dielectric Barrier Plasma Actuator: Geometric Effects.* AIAA Journal, 2004. **42**(3): p. 595-604.

[19] Enloe, C.L., et al., *Mechanisms and Responses of a Single Dielectric Barrier Plasma Actuator: Plasma Morphology*. AIAA Journal, 2004. **42**(3): p. 589-594.

[20] Santhanakrishnan, A., D.A. Reasor Jr, and R.P. LeBeau Jr, *Characterization of linear plasma synthetic jet actuators in an initially quiescent medium.* Physics of Fluids, 2009. **21**(4).

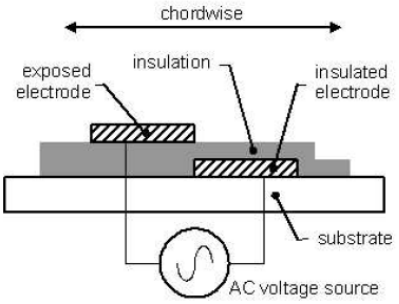

Figure 1 The plasma actuator in chord wise section.

$$\nabla.(\varepsilon_r \nabla \phi^*) = 0 \qquad \nabla \cdot (\varepsilon_r \nabla \rho_c^*) = \rho_c^* / \lambda_d^2$$

$$\rho_c^* = \frac{\rho_c}{\rho_c^{\max} f(t)}$$

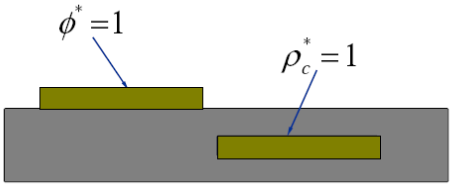

Figure 2: The non-dimensionalised simulation domain.

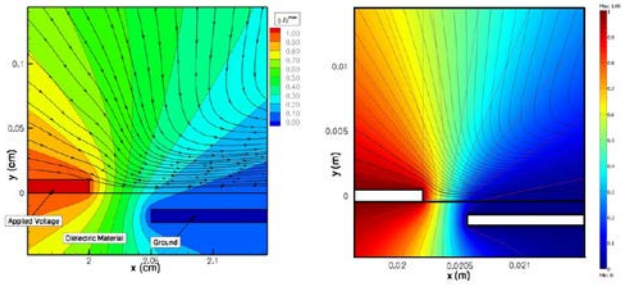

Figure 3 Comparison of the electric potential contours from simulations done in GHOST[10] and COMSOL.

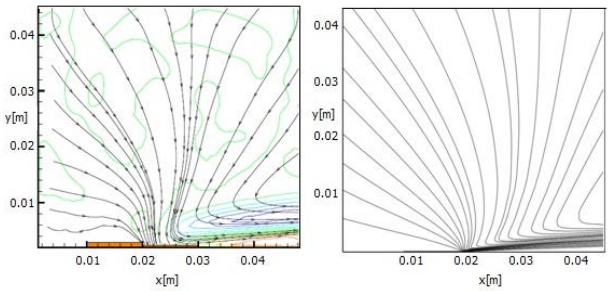

Figure 4 Quiescent flow streamline plots obtained from experiment [17] (left) and COMSOL (right).

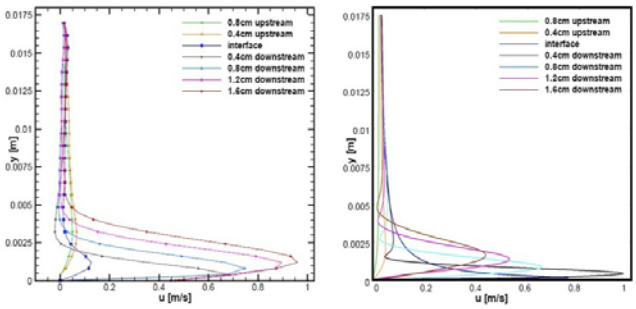

Figure 5 The u-velocity profiles of 8 stations taken from experimental [20] (left) and COMSOL (right) results.

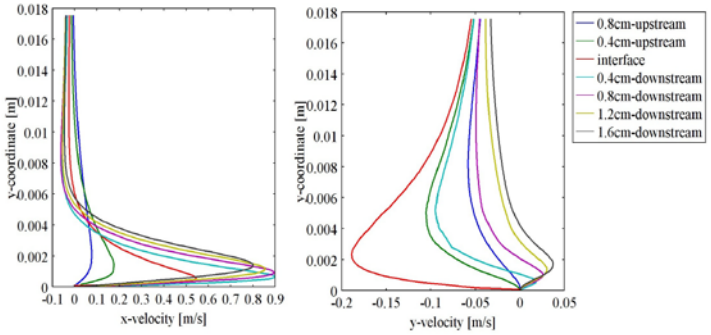

Figure 6: The u- (left) and v-velocity (right) profiles for the tuned parameters with tuned parameter

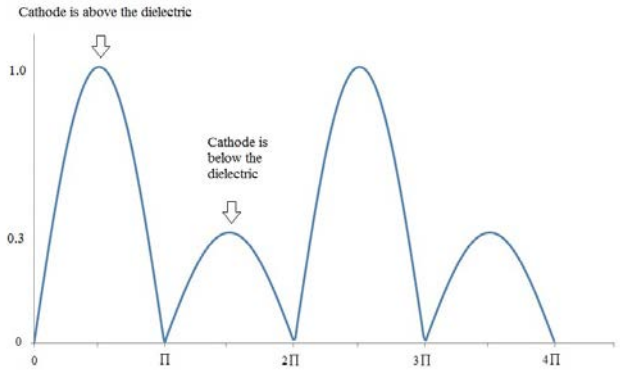

Figure 7: Two cycles of equation (38) showing the positive and negative non-dimensionalised charged density waveforms.

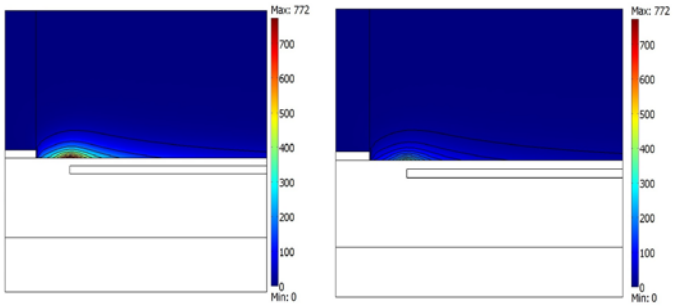

Figure 8: The resulting positive (left) and Negative (right) waveforms non-dimensionalised body forces.